

HYSPEC Status, June 30, 2013

On February 5, 2013, we provided a status report on the HYSPEC instrument; this is a quick follow-up report on each of these issues.

1. User program for unpolarized neutrons

Ovidiu Garlea is now an instrument scientist on HYSPEC. He comes most recently from the HB2A Powder Diffractometer at HFIR, and before has been instrument scientist at HB1 and HB1A.

In the Spring 2013 call for proposals, ORNL received 22 requests for beamtime through the user program. Of these, nine successfully went through the Science Review Committee (SRC). Because we successfully ran many of the sample environments this spring, that we expect to use in the user program, we don't expect to see as many proposals diverted to instrument development in the future.

The IDT time allotted for the Fall 2013 cycle is 16 days. Please let us know which experiments the IDT would like to run. The IDT agreement for HYSPEC is being drafted at ORNL, as the first of a new set of standardized agreements, and will be released to the IDT for comment and negotiation shortly.

Several attempts to use high incident energy (60-90 meV) have proven unsuccessful over the last three cycles, due to low flux, so we are restricting HYSPEC's incident energy range to 3.8-60 meV.

We continue to reserve beamtime for polarization analysis instrument development, and are for now not accepting proposals that require polarization analysis. However, we do already have limited polarization analysis capability, and would like to perform an experiment demonstrating this capability during our instrument development time this fall. Please contact Ovi or Barry if you have an experiment in mind.

The race has begun in earnest, to see who will publish first with HYSPEC data! For those of you preparing for publication using HYSPEC data, we encourage you to use the following text in your acknowledgement:

[Part of the] Research conducted at ORNL's Spallation Neutron Source was sponsored by the Scientific User Facilities Division, Office of Basic Energy Sciences, US Department of Energy.

and please refer to the HYSPEC instrument directly when describing your experimental procedure.

2. Polarization commissioning

Previous status:

For incident beam polarization using the Heusler focusing array, initial characterization was achieved using 3-He cells and a moderate-quality Heusler single crystal. For flipping of the incident beam, the prototype Mezei flipper worked but we had begun preparing for an improved design. For polarization analysis using 3-He cells, the 3-He was polarized in the lab and transported to the Helmholtz-like coil system for several tests, including a vanadium scatter flip vs. no-flip demonstration, using a cell not optimized for ~15 meV transmission. For polarization analysis using the supermirror polarizing array, the agreement between PSI and ORNL was in process, and the magnetizer was being redesigned.

Update:

In February, we tried two cells, and again measured spin-flip vs. no-spin-flip scatter from vanadium. The table below shows the parameters and results. In the calculation, we assume the neutron polarization is 90% and the flipping efficiency of the Mezei is 10. The main advantage of the Barbera cell measurement over last fall's, is that the 3He pressure and size of these cells was better suited for 15 meV Ei, and permitted much more rapid data acquisition. The Melbac cell measurement was limited because the cell was not thoroughly polarized prior to transport to HYSPEC.

Cell Name	Pressure (bar)	Length (cm)	3He Polarization	Measured Ratio	Calculated Ratio
Barbera	1.52	8	70.9%	0.7118	0.60
Melbac	1.47	10	28.2%	0.8159	0.71

The prototype Mezei flipper control was automated, with direct control from the PYDAS data acquisition system. This permitted us to scan flipping current and to script overnight data acquisition.

Initial testing of the 5 T vertical bore magnet Slim SAM revealed that the vertical guide field in the drum shield exit port needs to be inverted, because the polarity of Slim SAM could not be reversed. This activity is planned for the winter outage in early 2014. Other magnets at the SNS (FAT SAM and the in-procurement FIT-SAM) have reversible polarity.

We moved power supplies for the Mezei flipper off the experiment floor, to a rack above the drum shield, but found the maximum current was too low due to the extra length and small conductor size. Both of these limitations are being addressed this summer.

Parts for the new Mezei flipper have been fabricated, and a test assembly without winding was successful. Winding of this new flipper is planned for this summer.

For polarization analysis using the ^3He refillable cell, the new titanium bellows for the syringe has been pressure tested and shipped to ORNL. Final post-check changes to fabrication drawings for the syringe flange and valves, and for a dedicated custom cart, are underway; solicitation for bids for fabrication is immanent.

For polarization analysis using the polarizing supermirror array, negotiations with PSI are nearly finalized. The subcontract for final design and fabrication of the ORNL magnetizer has been awarded. The guide field design is being finalized.

3. New data acquisition system prototyping

The new event-based data acquisition system has been run in parallel with the legacy system for two cycles, and for short periods of time this spring, we were using the event-based system exclusively. We expect to be using only the event-based system starting in the Fall cycle. New developments this spring include easier live viewing using Mantid on the HYSPEC analysis computer and Analysis cluster; scan improvements that enable reconstruction of rocking curves, etc. using Mantid; storage of HYSPEC runs on a faster-access parallel file system; chopper TDC logging in the nexus files for better filtering via Mantid; an ADARA system status watcher called DASMON that is now on display at HYSPEC's control room, and which can be run from the HYSPEC analysis computer and Analysis cluster; and the ADARA status webpage. Rollout of this new system to some other instruments at the SNS is beginning at the end of the spring 2013 cycle.

For both the old and new systems, we have been generating autoreduced files this spring, which are readable by both DAVE's MSLICE and HORACE. This system automatically selects the best window for time independent subtraction for a given incident energy. The files come in two grouped formats: one that bins each detector tube into 32 subsets, permitting limited vertical Q resolution; and one that bins a full detector tube into a single subset, but masks the top and bottom quarter, so that the sensitive region matches the divergence from vertical focusing.

4. Prompt Pulse Background

Previous status:

A time dependency to the prompt-pulse feature was found to be caused by the opening of the BL 13 secondary shutter. A facility wide shutter test determined that the bulk of the background remains when all shutters are closed. Gradual time variations in the background feature remained unexplained.

We have not pursued additional shielding strategy/tests to mitigate the BL 13 secondary shutter, whose opening and closing has complicated efforts to employ empty can subtraction to remove the prompt pulse feature. However, they are no longer using the configuration that they claimed would most impact this background feature.

Update:

The portable detector array was disassembled for use elsewhere at ORNL. We know of a possible hot-spot atop BL-18 near the monolith, but have not attempted a shielding test there yet. We are planning to rebuild a high energy neutron detector in order to map the high energy neutrons in the fall.

An automated reduction routine has been prepared, that avoids the prompt pulse when selecting a time-of-flight range for time-independent background subtraction.

5. Other background

Previous Status:

Scatter from air, the drum shield, optics upstream of the sample, sample environments, and the detector vessel have been minimized using a crude prototype shield about the sample. Based on lessons learned from making this prototype, and using feedback from both ORNL staff and friendly initial users, we have designed a more permanent shielding solution.

Update:

The new beam stop has been in use since early April, and its motorized translation has made optimizing position for maximum angle coverage and minimum background much easier. The new cover for the fine radial collimator has been in use since late March. The new pre-sample shielding will be fitted with neutron absorbing material during the summer shutdown, and will be ready for use during the fall cycle.

Several of our users have experienced problems with what seems to be intense Bragg scattering from the sample, seeming to scatter again after the fine radial collimator. A temporary solution employed by one user team was to apply a temporary absorber where the Bragg scattering hits the entrance window. We are currently trying to better characterize this background feature.

6. Detector vessel location, motion and collision avoidance

Previous status:

Mostly fixed, and spares in hand.

Update:

Sonic sensors at the back corners of the detector vessel were reoriented to improve collision avoidance. A light curtain system has been purchased and will be installed at both the western wall and the equipment lift cage.

The swinging arm on the drum shield, which is opened for 3.8 to 7 meV Ei but closed at higher Ei, was prevented from opening in March because a safety pin would not engage properly. The motion

of that safety pin was hindered because one of the linear stages had gotten misaligned after repeated use. This stage remains in place but is now loosely connected; other stages permit reliable motion now. We have used the swinging arm and pin system several times since without incident.

This summer we will install an encoder for the pinion (a more direct measure of drum shield angle), and an angle indicator at the bottom of the drum shield, to more easily recover from the rare events where we lose drum shield angle information.

7. Recent activity with sample environments

Previous status:

Larger diameter tails for CCR's were built and used, and a 450 K sapphire standoff was installed on CCR-10 for use in an inelastic powder experiment.

Update:



Figure: Slim SAM (5 T, vertical bore) at HYSPEC

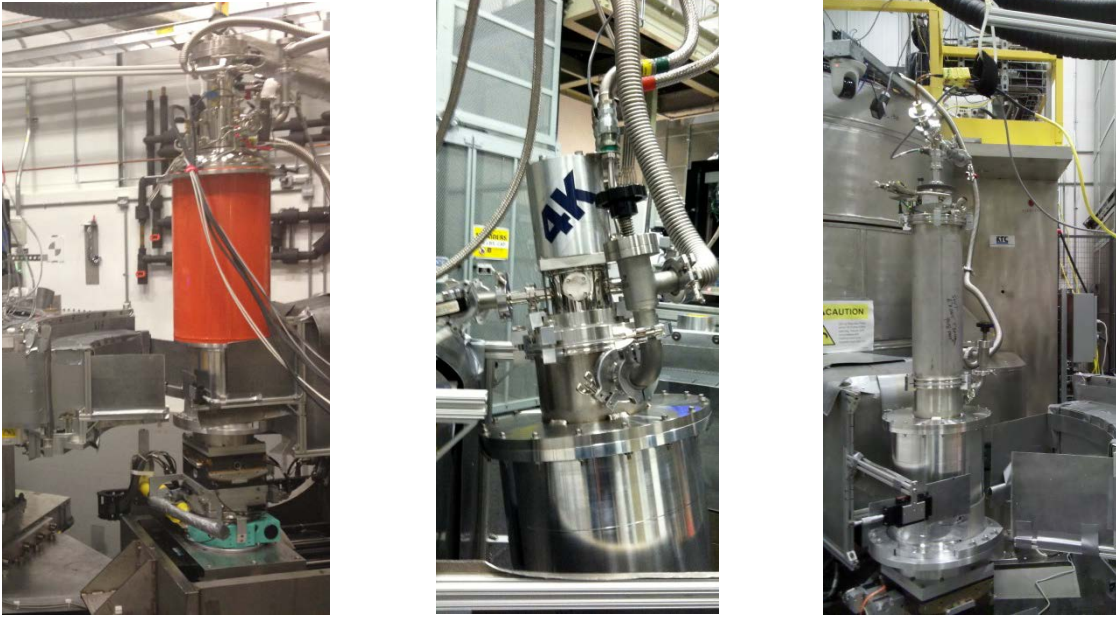


Figure: Left to right: Dedicated orange cryostat CRYO-09, High T CCR CCR-10, and ARCS furnace stick HS-01 in the CCR-10 tail.

The dedicated orange cryostat has been used to cool down samples in an experiment at HYSPEC. A 3-He insert for this cryostat, which reaches lower temperatures, is currently in procurement and will hopefully be tested in the spring of 2014.

CCR-10 has been fitted with a 700 K sapphire switch and used at HYSPEC in May 2013. CCR-10's tail has an adaptor for an ISO-160 flange with taller stick. This adaptor was used with the ARCS furnace stick, also to reach 700 K.

SLIM SAM has been used at HYSPEC, up to 5 T. It can only run at one polarization, which is unfortunately oriented opposite to our guide fields. Plans have begun to invert our guide fields.

The Janus Cryostat CRYO-01 has been used at HYSPEC, both with and without the 3-He insert ULT-01.

8. Recent activity, general performance

Previous status: the major leak that was found to be under the downstream chopper racks was left alone, due to expected 2 month downtime and continuous work. Disk choppers were tested and found to function up to higher pressure. Pressure dropped in spring of 2012 to ~ 70 mTorr. In the fall of 2012 the pressure rose again to ~ 250 mTorr

Update: Pressure this spring is currently stable at ~ 200 mTorr.

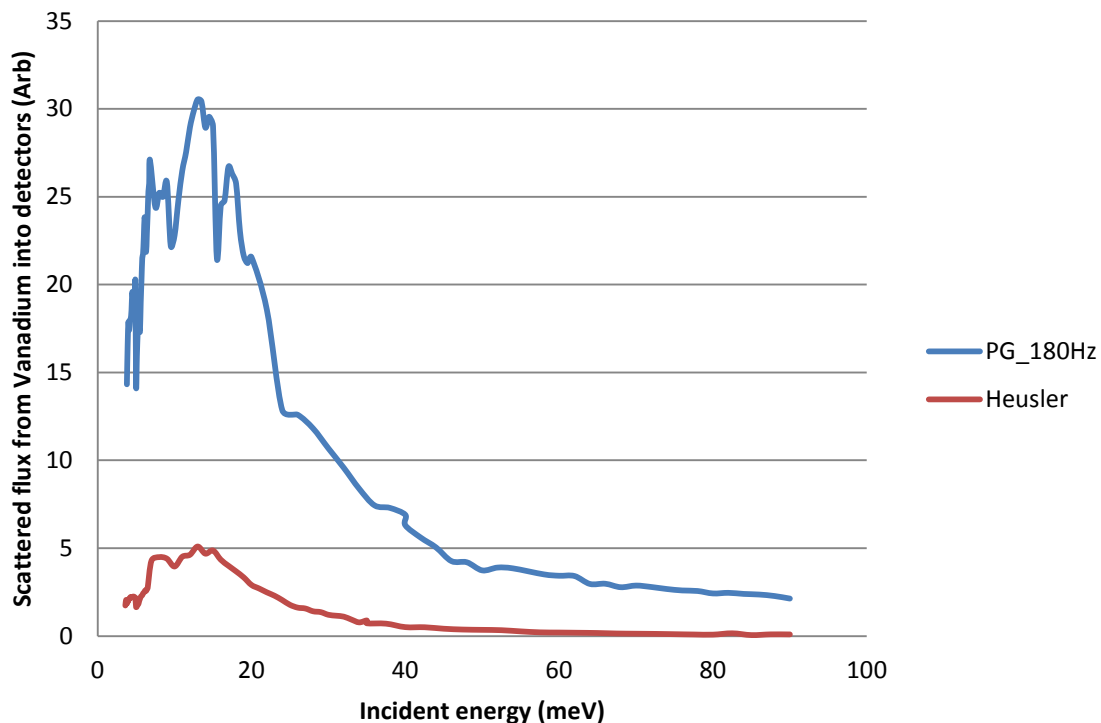
Previous status: we were preparing python routines to aid in planning experiments.

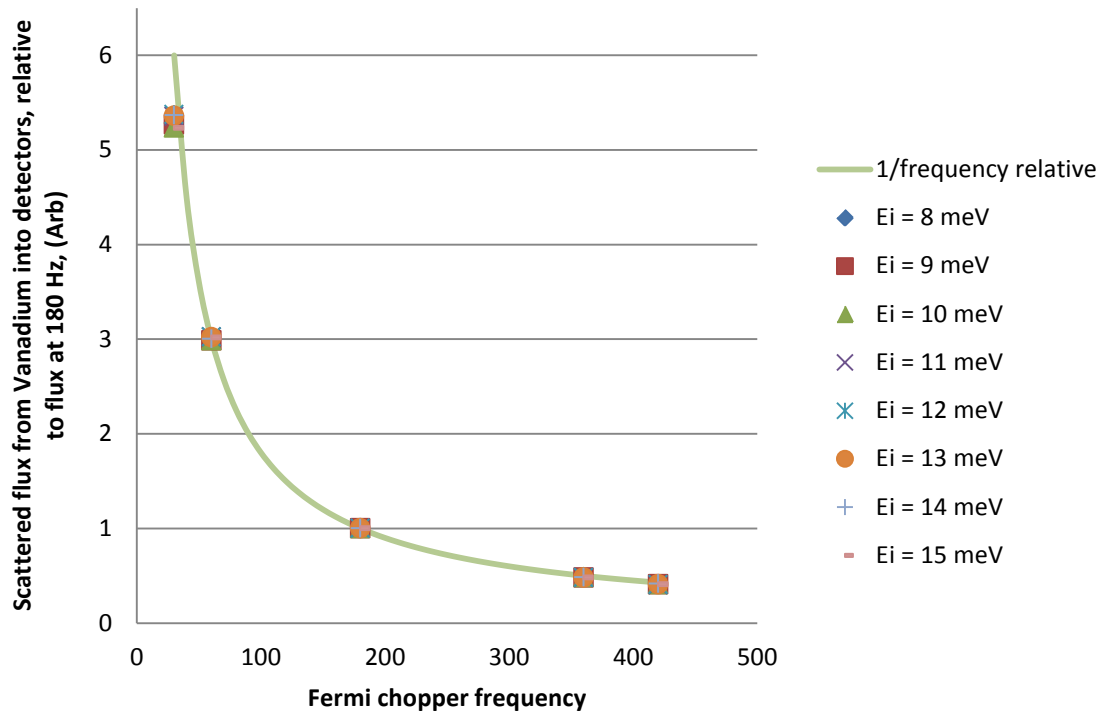
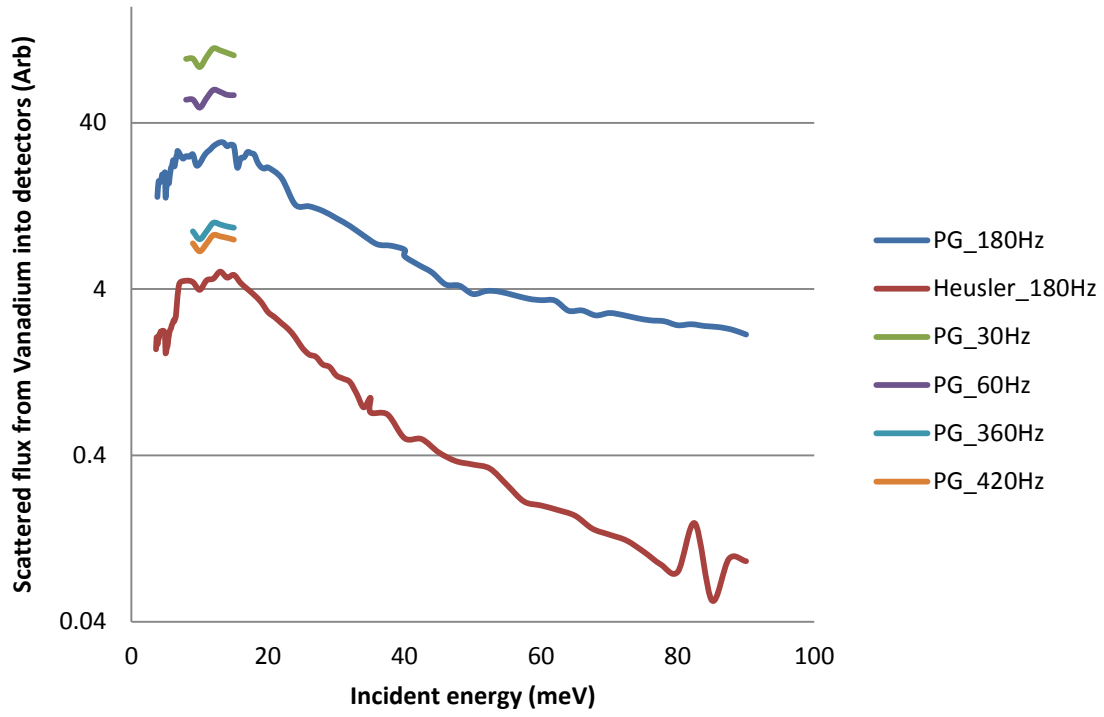
Update: these planning tools have been used by several users this spring, on both PYDAS and in an ipython shell on the Analysis cluster. A tutorial on how to use these tools is available upon request.

9. Flux and resolution characterization with vanadium

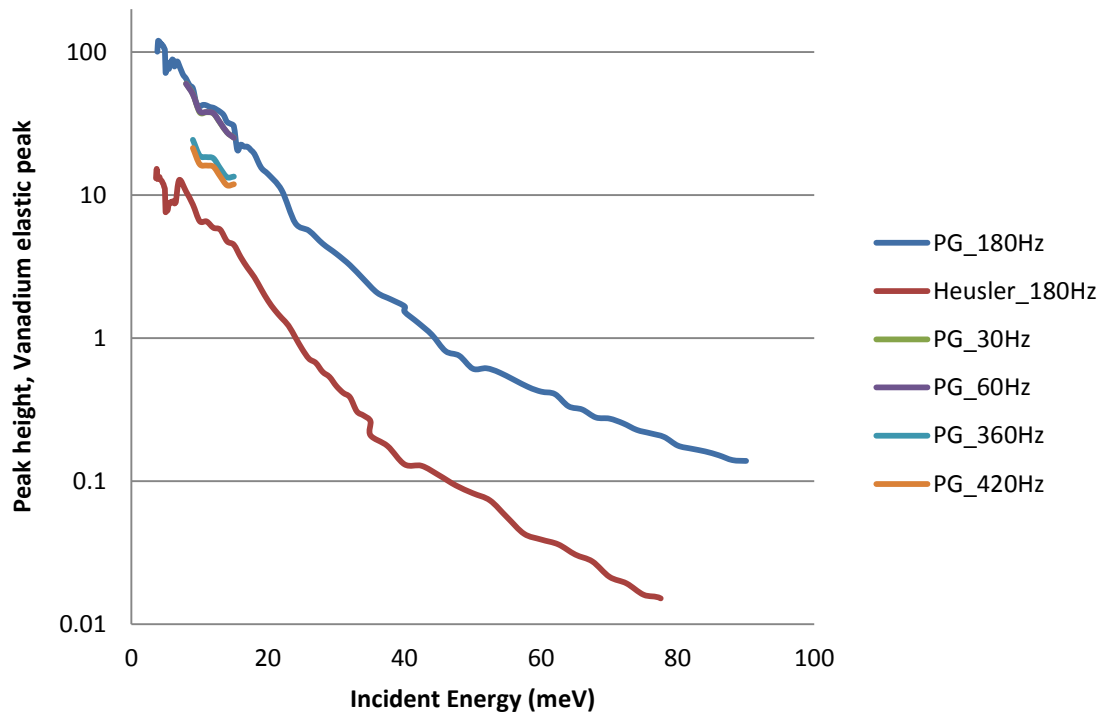
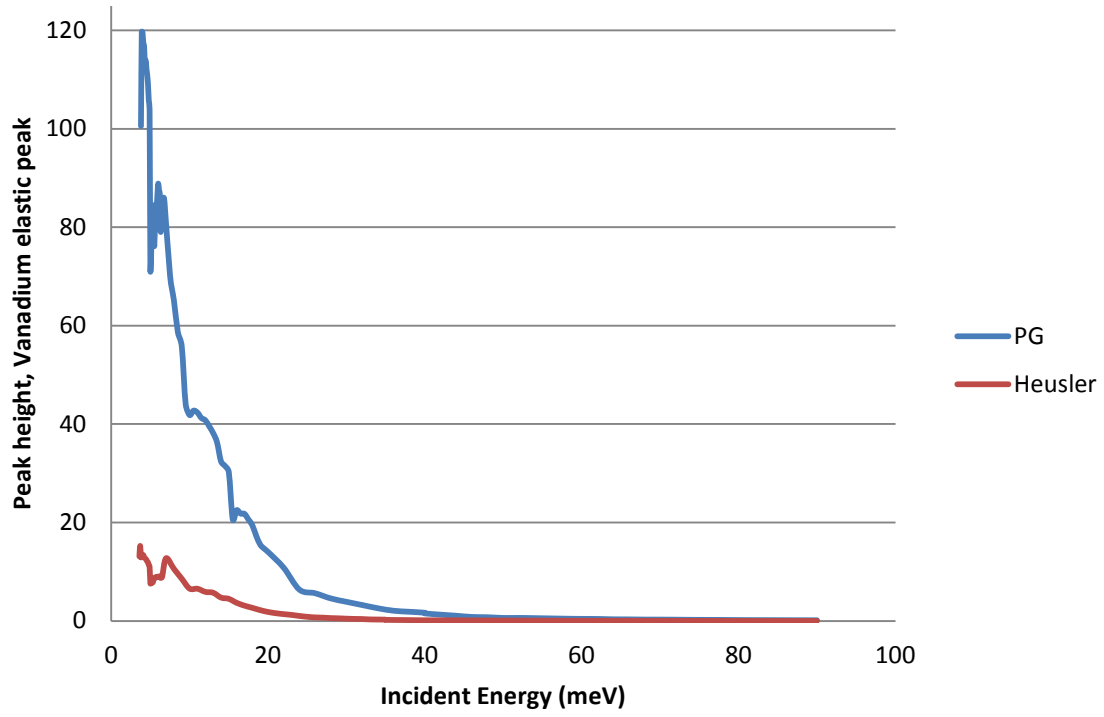
Measurements were made for a large number of incident energies, using a 6 mm diameter vanadium rod in air, using both the PG and the Heusler focusing elements. In a more limited incident energy range, we have also measured at a range of Fermi frequencies using the PG focusing element. These measurements were taken prior to finding a bug in the set_Ei python routine, so that the Fermi phase was not correct for the nominal E_i; E_i's were therefore determined during reduction as a function of the Fermi phase. Documents have been prepared with individual spectra plotted with Gaussian fits to the elastic line, which are available upon request. Below are plots associated with these measurements.

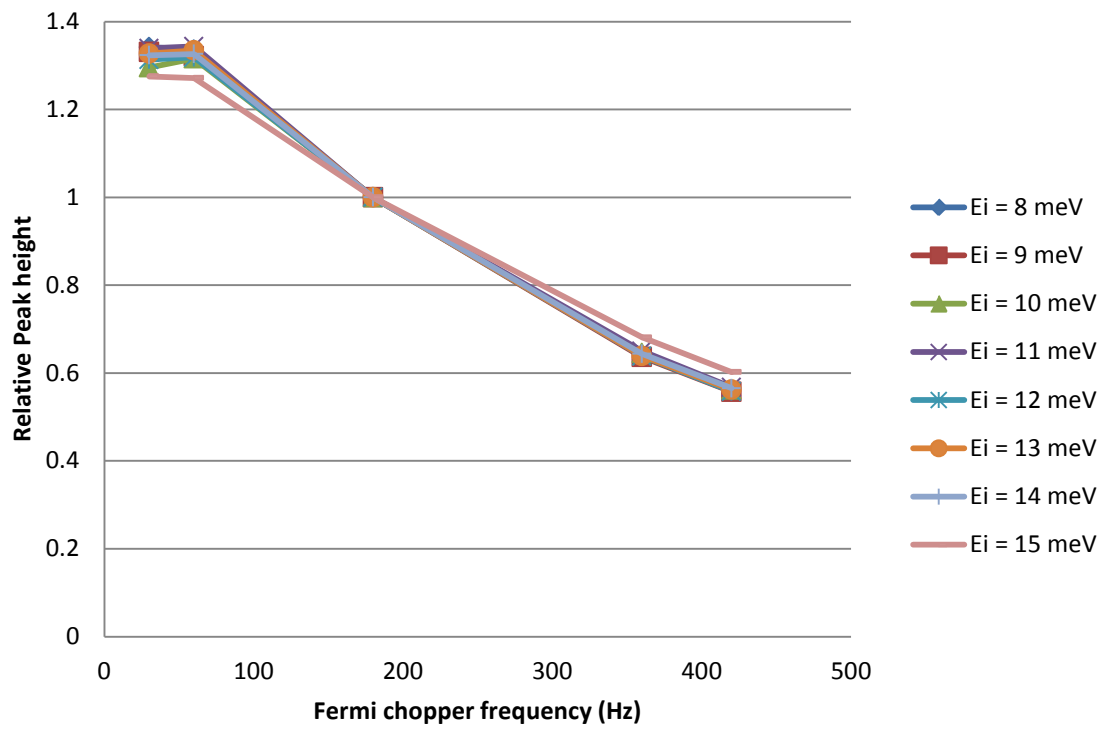
Integrated Flux:



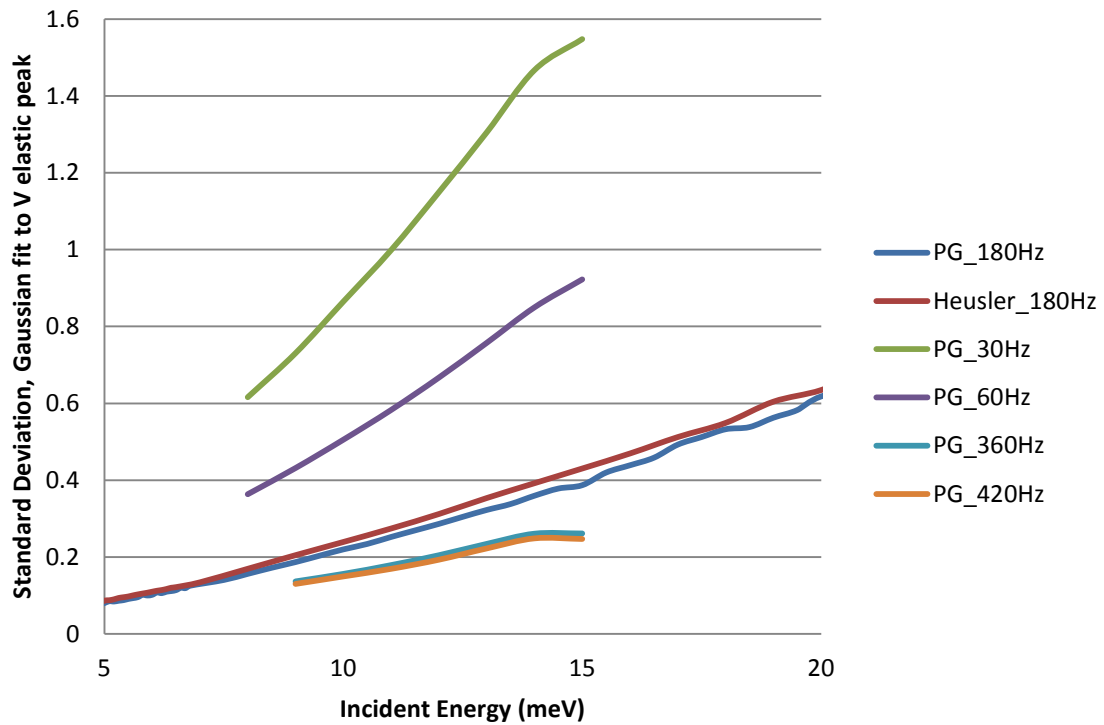
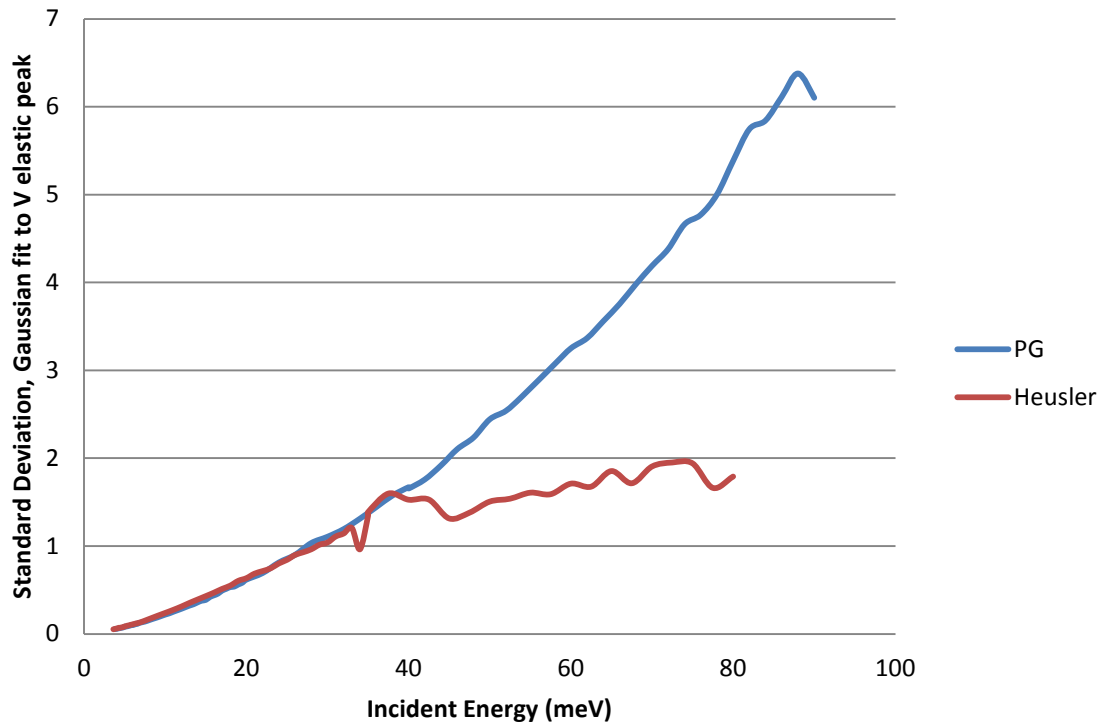


Peak flux:

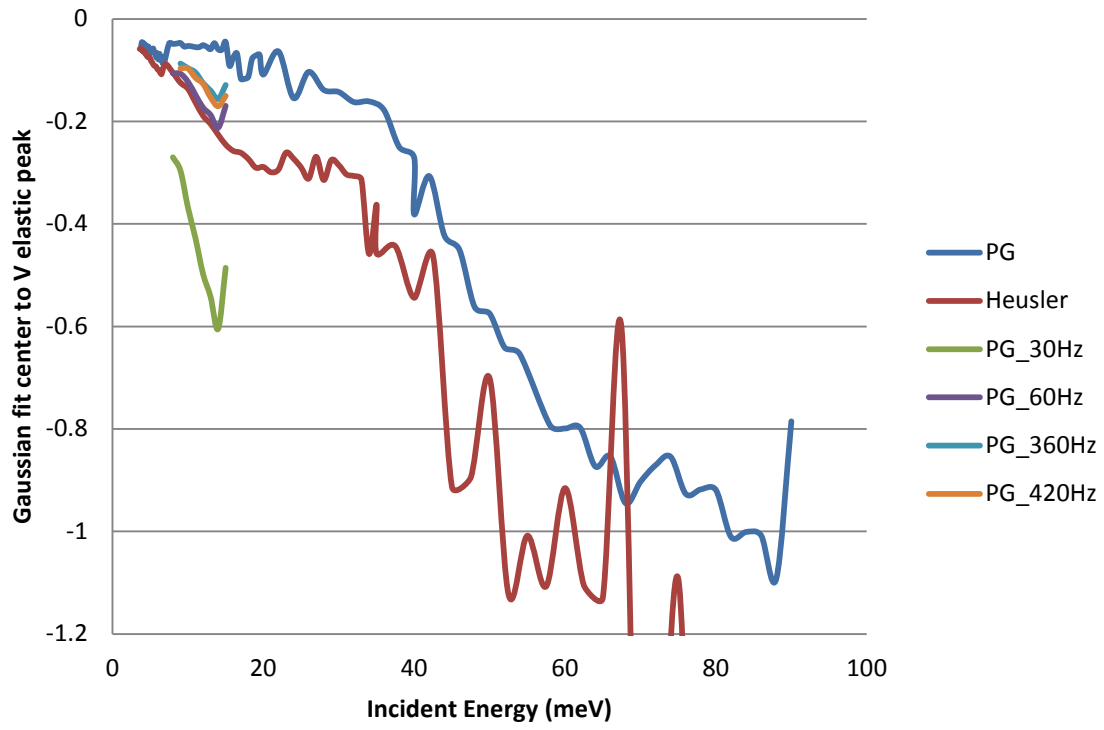




Standard Deviation of elastic peak:



Position of elastic vanadium peak:



10. Recent activity with users

I. Zaliznyak: FeSb_2 (IPTS-8361, January 2013)

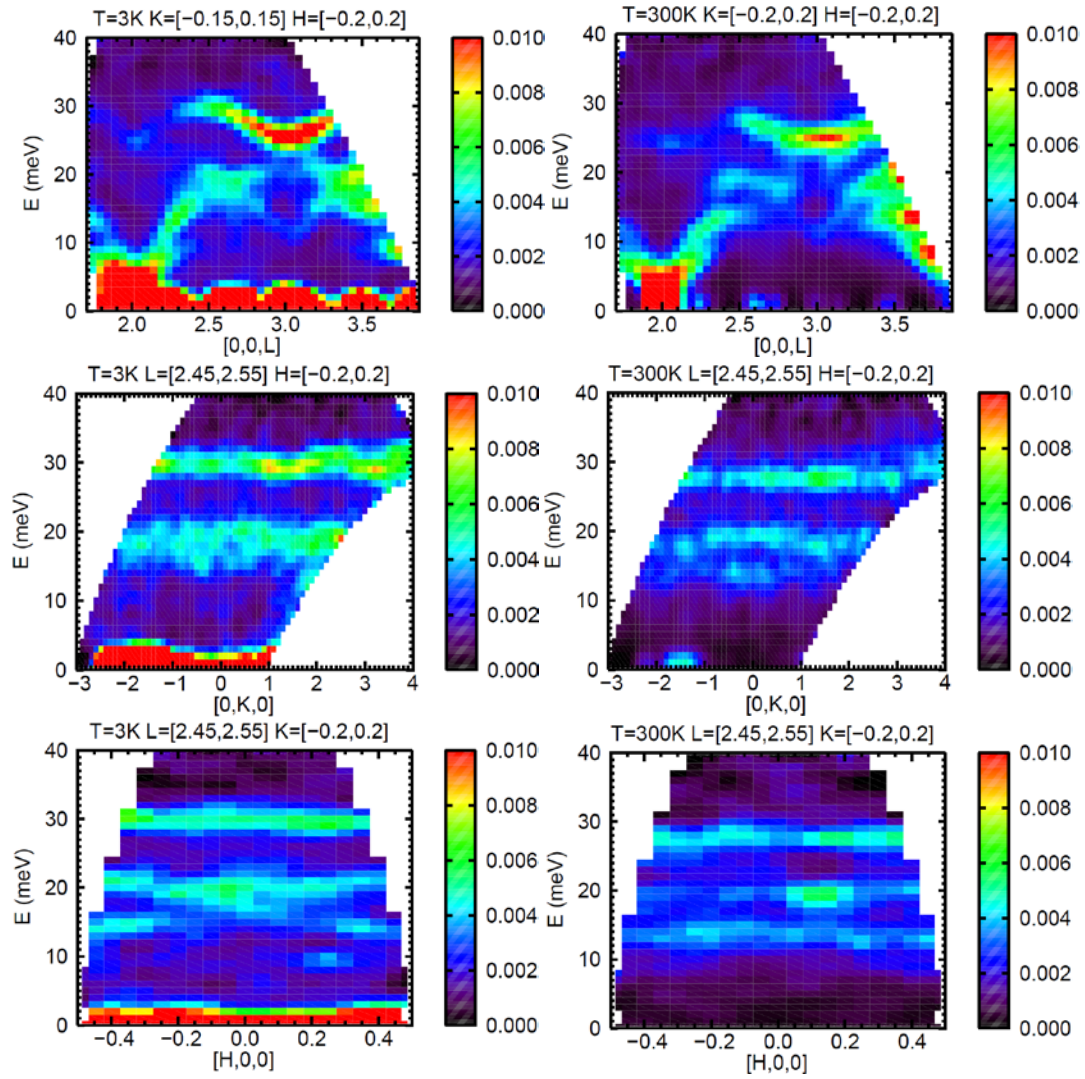


Figure: Electron-phonon anomalous softening in quasi-one-dimensional narrow-gap semiconductor. $E_i = 51$ meV. Each dataset is approximately 24 hours on HYSPEC: 1/2 hour for each of the 46 angular positions of the sample.

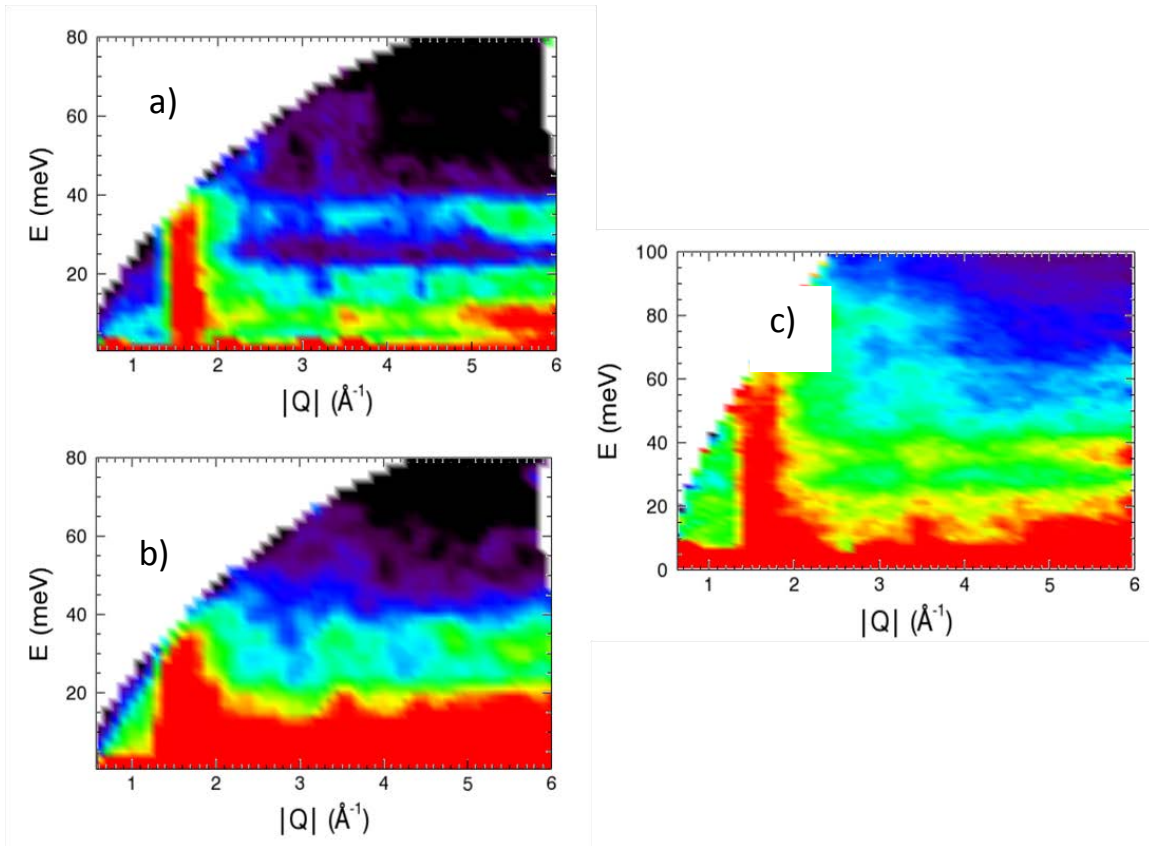


Figure: (a) Inelastic neutron scattering data measured at HYSPEC with incident energy 90 meV at 5 K and (b) 450 K (bottom), (c) Inelastic neutron scattering data measured at SEQUIOA with incident energy 250 meV at 5 K

LaMnPO, isostructural to the iron pnictide superconductor LaFePO, is an antiferromagnetic insulator with $T_N = 375$ K. We used HYSPEC to measure high energy magnetic excitations in LaMnPO and to study the temperature dependence of these excitations. To achieve the largest energy transfers while also accessing the lowest momentum transfers, the highest possible incident energy of 90 meV was used and the detector was moved to the lowest angles. At 5K (Fig. 1(a)) the most prominent feature is the pillar of scattering centered at 1.6 \AA^{-1} , coincident with expected magnetic excitations emerging from the (100) Brillouin zone center. These excitations extend up to at least 40 meV suggesting the exchange interactions are strong in this material. When the temperature is increased to 450 K (Fig. 1(b)), well above the ordering temperature, the same magnetic excitations are still present. Figure 1 (c) shows the same material measured at 5K on the SEQUIOA instrument. The pillar of scattering centered at 1.6 \AA^{-1} is the same as that measured at HYSPEC. This experiment emphasizes the persistence of exchange coupled spins in the paramagnetic state of LaMnPO, an observation also made in some of the iron pnictide superconductors.

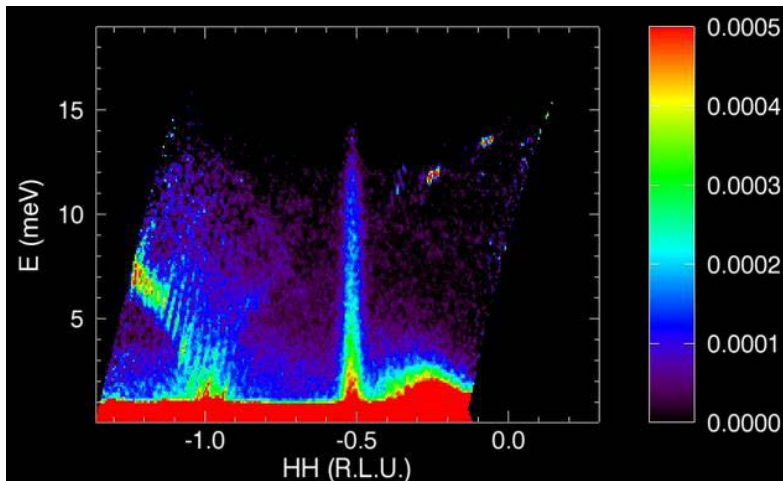


Figure: Energy vs. wave vector map obtained in the previous HYSPEC commissioning experiment. Since the magnetic excitations in this system are two dimensional, we integrate over a large range of the orthogonal L direction to improve statistics. This measurement was performed at 3.2 K and employs no empty cryostat data set subtraction.

The purpose of this experiment was to continue commissioning work on the HYSPEC spectrometer as well as to explore the magnetic excitations seen in $La_{2-x}Ba_xCuO_4$ (LBCO). There were two materials with different Ba concentrations measured in this experiment: $x = 0.025$ and $x = 0.0125$. The choice of the additional measurement of the $x = 0.025$ sample was to extend the measurements performed in the previous HYSPEC commissioning experiment from June of 2012. Further, as this was a commissioning experiment, the ability to compare this experiment's data quality to the previous measurement would be a good test of the reliability of the previous measurement. We also measured the $x = 0.0125$ sample to extend our study of the magnetic excitations in LBCO to a new material with a Ba concentration not measured previously. As well, this experiment was taken as an opportunity to test the new continuous rotation data collection method that had recently been introduced to HYSPEC.

We would first like to comment on the use of the new continuous rotation data collection method. From this experiment we found that this new method of data collection operates quite well and is no more difficult to use than the standard fixed angle data collection method. As will be seen, we were able to obtain high quality data from this experiment. While we have performed the current analysis in such a way as to bin the rotation data into effective 1 degree rotations of the cryostat, a power of this new method is that in future analysis we can control this rotation bin size to optimize resolution and statistics as our future analysis requires. This is a significant advancement over the standard fixed cryostat angle rotation method.

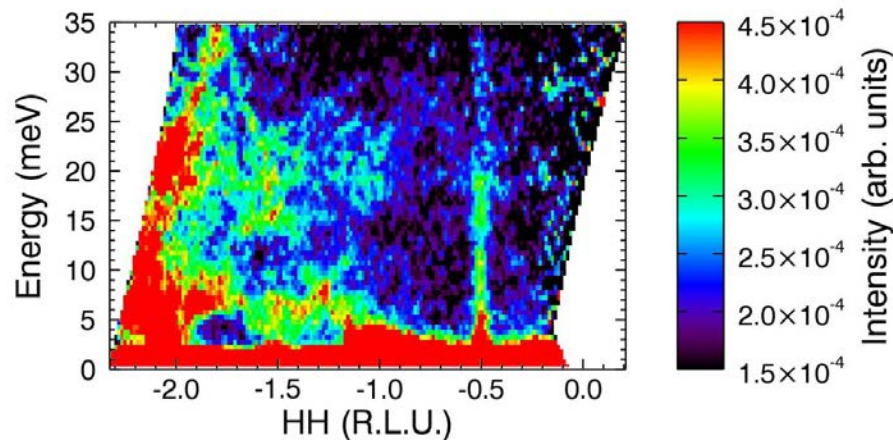
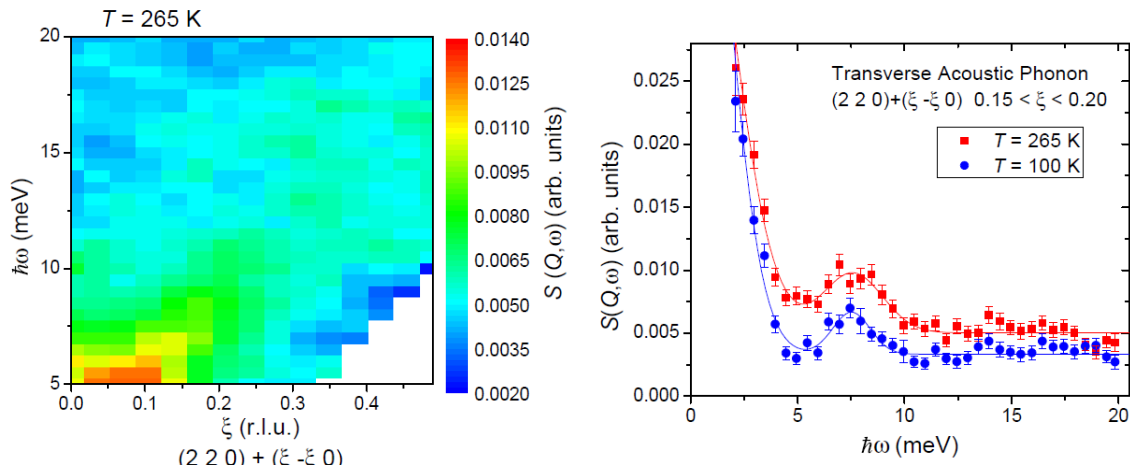


Figure: Energy vs. wave vector map obtained in the present HYSPEC commissioning experiment as performed on the $x = 0.025$ sample. A false 0 is chosen to better highlight the distinction between the magnetic signal and the background. This measurement was performed at 3.2 K and employs no empty cryostat data set subtraction.

Turning now to the data itself, the first figure shows an energy vs. wave vector map using data collected on sample of LBCO with $x = 0.025$. We note that this data was collected during the June 2012 experiment using neutrons with incident energy, E_i , of 20 meV. The magnetic excitation can be seen here as the relatively dispersionless feature extending out of the $HH = -0.5$ position. We are also able to resolve an acoustic phonon which extends out of the $HH = -1$ position. However, we were unable to measure to high enough energy at $HH = -0.5$ to observe the crossing of these two dispersive modes, which is a topic of interest in our group's research. This is because at the time of this measurement HYSPEC was only able to collect such high quality data with $E_i = 20$ meV.

In the second figure we show the same kind of energy vs. wave vector map as in figure 1, but now collected in the current experiment on the $x = 0.025$ sample at $T = 3.2$ K. Magnetic excitations can again be seen here as a highly dispersive vertical rod-shaped excitation extending from $HH = -0.5$. It is interesting to note that the scattered intensity seems to diminish above 20 meV, which appears to be consistent with our results from measurements on SEQUOIA. However, while this is a promising start to our analysis, during this experiment there were technical issues with one of the detector '8-packs.' These caused some of the detectors to incorrectly measure the time of flight of the scattered neutrons. At the time of this report, we have managed to correct for these effects in the data but have not yet applied similar corrections to a data set taken of an empty cryostat to remove the effect of the sample independent background. This will be of particular importance here since aluminum has a well-known phonon at 20 meV.



This sample is a well-known colossal magnetoresistive material with a combined metal-insulator and ferromagnetic transition at $T_c = 257$ K. It is known that structural polarons also play a role in the material's behavior at this transition, so we have been interested in phonons and other nuclear scattering near T_c . We took data on HYSPEC at 100 K (well below T_c , mostly to serve as a background) and 265 K (a bit above T_c , near where the polaron scattering intensity peaks) with the spectrometer roughly centered near the $(2\ 2\ 0)$ position which is a strong nuclear peak. The first figure shows a slice in Q-E space at 265 K. It clearly shows transverse acoustic phonons coming out of the peak, but they are pretty broad - particularly the scattering at energies below the phonon branch is pretty strong at q values up to at least $(0.25\ -0.25\ 0)$ away from the Bragg peak (incidentally, this is also the q position where the elastic polaron scattering is optimized). At higher energies there is also an optical phonon branch, but it is hard to see with the statistics from this experiment. I particularly like the second figure, showing an energy scan at both 100 K and 265 K. The phonon branch is located at roughly the same energy at both temperatures and the ratio in integrated intensities is as expected from the Bose factor. But interestingly, at 265 K the phonon shows more damping, and while the overall background is higher this is particularly true with some extra (maybe quasielastic?) scattering being present in the 265 K data at energy transfers between the elastic peak and the phonon. This is also largely consistent with what we saw on ARCS; I hope to do some triple-axis measurements soon on BT7 to see the temperature dependence a bit better.

D. Ye: PrFeO_3 (IPTS-8839, February 2013)

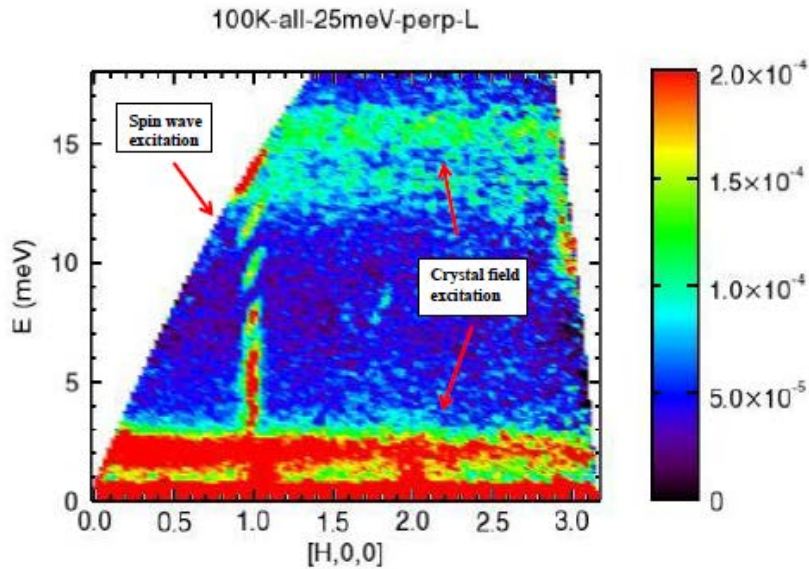


Figure: The spin wave excitation, measured on Hyspec at 100 K, is viewed perpendicular to [00L] direction; Incident energy is 25 meV and energy transfer was scanned at (101) reflection up to 14 meV. Three q-independent crystal field excitations have been observed at 2 meV, 13 meV and 15 meV energy transfer.

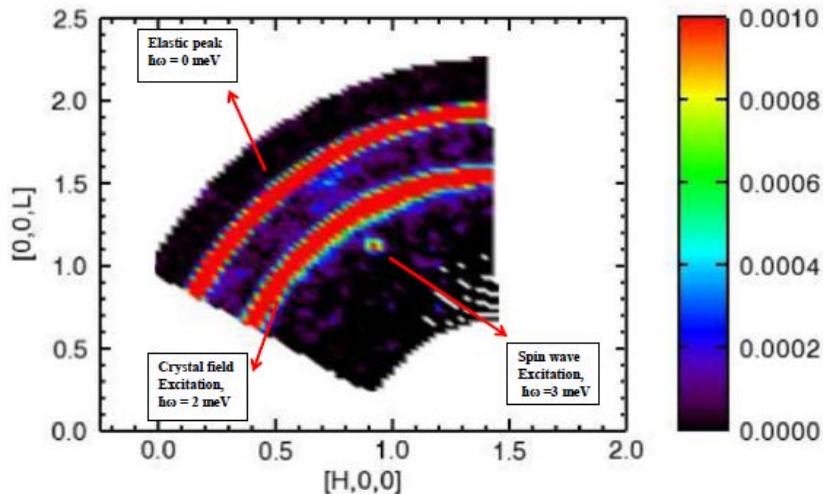


Figure: Inelastic neutron scattering was performed on single crystal PrFeO_3 using Hyspec instrument. Incident energy is 6 meV and sample temperature is 5 K. Crystal field excitation was observed at 2 meV energy transfer. Spin wave excitation was detected at 3 meV energy transfer along (101) direction.

D. Fobes / I. Zaliznyak: Fe1.1Te (IPTS-8012, March 2013)

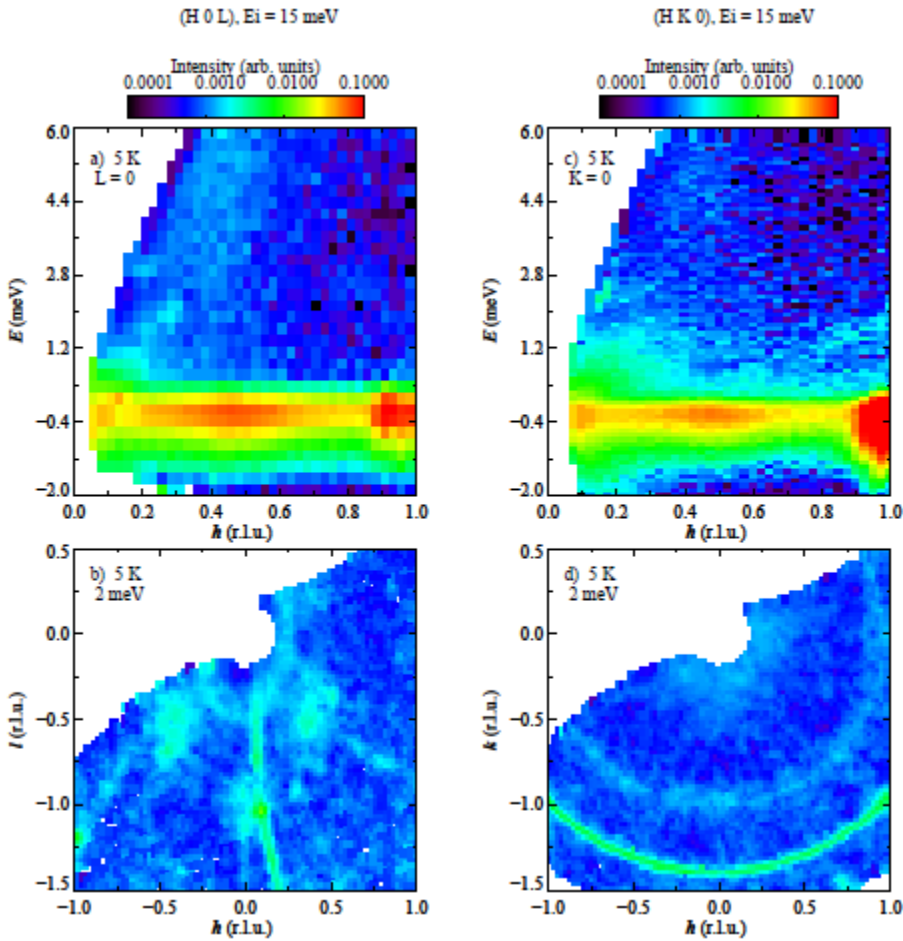
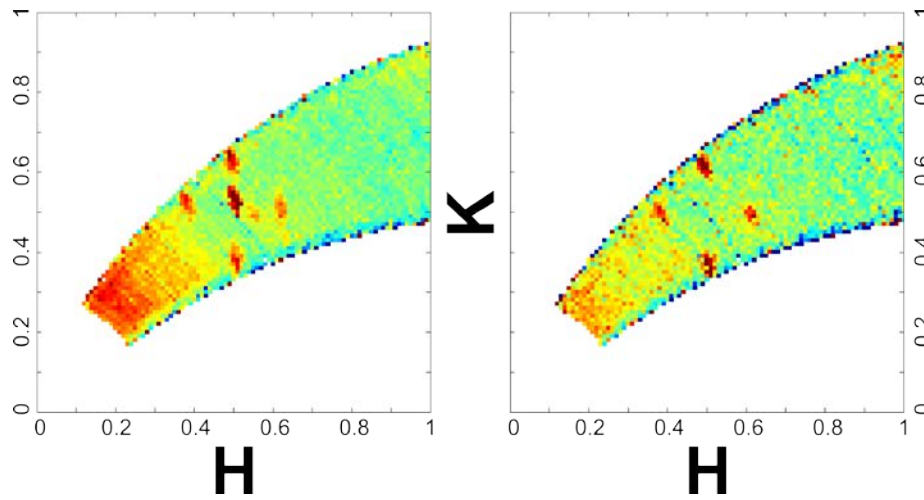


Figure: Inelastic slices in the (H 0 L) (left column) and (H K 0) zones (right column) at 5K with $E_i=15$ meV. (a) and (c) show the energy dispersions at $L=0$ and $K=0$ taken in the two different sample configurations. (b) and (d) are inelastic slices at 2meV in the two sample configurations. We do observe a mode which seemingly emerges from $q=0$ in the (H 0 L) zone (a) and (b), but is contaminated by the presence of contamination from re-scattering of Bragg scattering. No similar mode is obviously present in the (H K 0) zone.

The goal was to search for a low energy acoustic mode which appeared to approach $q=0$ (Zaloznyak et al., PRL 107, 216403 (2011)). These measurements were inconclusive; we have not been able to observe a feature that clearly corresponds to the mode observed at ARCS, and features that may correspond are not consistently observed between different sample configurations. Spurious features are still abundant in measurements. In particular in this measurement, we observed contamination in runs that contain Bragg peaks (e.g. the radial stripe through (0,0,1)), which seems to arise from re-scattering of the strong Bragg scattering in this sample. Additionally, we encountered some contamination at low angle that necessitated some cutting of the signal at the first detector, which may be partially solved by the newer beam stop. However, the generally cleaner low angle range is the immediately obvious benefit over ARCS. Solving these issues and obtaining more intensity in the region of interest will be necessary.

D. Reznik / J. Tranquada: LBCO (IPTS-8359, March 2013)



The purpose of IPTS-8359 was to study the energy- and temperature-dependence of the spin density wave (SDW) and associated charge density wave (CDW) in LBCO. The SDW satellites, which form rods near $[0.5, 0.5, L]$, can be clearly resolved (see figure). The signal at $[0.5, 0.5, 0]$ (left panel) is due to multiple scattering, but HYSPEC affords us the versatility to simply integrate from $L = -1$ to -0.3 , removing this contamination (right panel).

We were also able to resolve the CDW at low temperature, although unfortunately the feature fell partially on a gap in the detector bank. We were unable to conclusively resolve the charge dynamics, in part due to additional background generated by a new form of spurion particular to HYSPEC (multiple scattering from a Bragg peak incident on the detector tank window). We have developed a workaround to reduce that spurion (using Cd strips as a mask to block the Bragg peak), and hope repeat the experiment in the future, armed with this new understanding.

Feedback for future development:

- 1) Some scripts supplied as templates for automated data acquisition crashed the DAS system.
- 2) The detector gaps can be tricky- about half of our peak fell into one of those gaps (at least at elastic energy; it may still be OK for the finite-transfer data). The experiment-planning software (used for checking the S_2 angle) does not show those gaps, which may be worth including in the future. Somewhat related- is it possible to combine two datasets collected with different S_2 angles? If so, the gap could be handled by taking a dataset, rotating the S_2 angle by some amount (say, half the distance between gaps), then taking more data.
- 3) New kind of spurion- some sort of multiple scattering from the aluminum window at the front of the detector tank produced some extra background near the 200 peak. Our solution was to place a strip of cadmium in front of the aluminum window, such that it blocked the incoming 200 Bragg peak. This reduced the background, but combining these data with the unmasked data needs to be handled carefully.

F. Ye, S. Chi: Magnetic dynamics in the honeycomb lattice Na_2IrO_3 (IPTS-8718, March 2013)

The honeycomb lattice Na_2IrO_3 has inspired a great deal of experimental and theoretical interest as it was predicted to be a possible topological insulator [1-3]. However, discrepancies among various theoretical proposals and experimental observations clearly point to the lack of a much-needed characterization of the magnetic and crystal structures of the honeycomb lattice [4, 5]. Our single-crystal neutron diffraction study has filled this gap by conclusively determining the crystal and magnetic structures of the Na_2IrO_3 [6]. To further understand the nature of zigzag magnetic state, we have used inelastic neutron scattering (INS) to investigate the interactions of the magnetic spins within the honeycomb planes and the corresponding effective Hamiltonian. A recent INS study at ISIS has provided evidence of significant long-range Heisenberg exchange interactions J_i , in addition to the highly anisotropic Kitaev term K . However, the poor statistics of the reported measurements prevent a quantitative analysis of the relative strength [7]. The preliminary study using HYSPEC on the powder sample (See Figure) would enable a conclusively determination of the dispersion relation, and understand the microscopic interactions responsible for the exotic zigzag spin order.

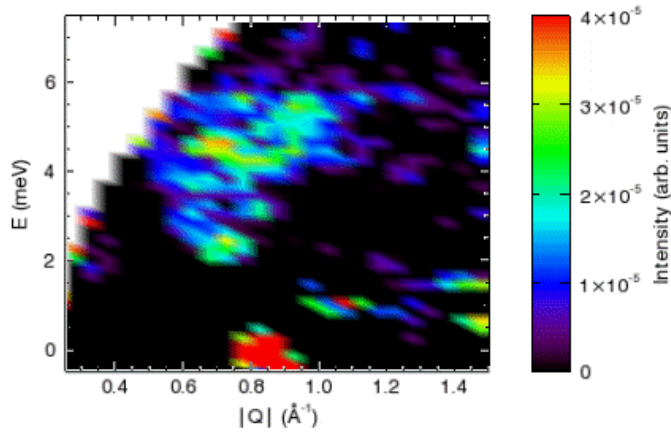


Figure 1: The spin excitation of the Honeycomb lattice Na_2IrO_3 measured with $E_i=15\text{meV}$ at $T=1.5\text{K}$.

- [1] A. Shitade *et al.*, Phys. Rev. Lett. **102**, 256403 (2009).
- [2] Y. Singh *et al.*, Phys. Rev. Lett. **108**, 127203 (2012).
- [3] D. Pesin, and L. Balents, Nature Physics **6**, 376 (2010).
- [4] Y. Singh, and P. Gegenwart, Phys. Rev. B **82**, 064412 (2010).
- [5] H. Gretarsson *et al.*, Phys. Rev. Lett. (2013).
- [6] F. Ye *et al.*, Phys. Rev. B **85**, 180403 (2012).
- [7] S. K. Choi *et al.*, Phys. Rev. Lett. **108**, 127204 (2012).

O. Garlea: Crystal field excitations in delafossite systems $RCuO_{2+x}$ (IPTS- 8945, March 2013)

The $RCuO_{2+x}$ materials, obtained by oxygenation of delafossite-type compounds, conserve the layered nature of the parent structure, with “x” values of the extra oxygen content up to $x= 1/2$ for $R=Y$, and $x= 2/3$ for $R=La, Nd, Eu, Pr$. Due to the presence of triangular arrays of spin $1/2$ Cu^{2+} cations with antiferromagnetic interactions, these materials can act as model compounds to study the effects of topological magnetic frustration in two-dimensional systems. The $x = 2/3$ concentration is particularly interesting since the structure shows a Cu network which is topologically equivalent to the kagomé lattice, where the magnetic ions sit on the vertices of corner sharing triangles.

The main goal of the experiment was to measure crystal-field excitations for the delafossite compounds with $R=Nd$, to improve the understanding of the differences in the magnetic behavior of the parent $NdCuO_2$ and doped $NdCuO_{2.66}$ systems. At the same time, this experiment was meant to serve as a test-bed for using the CRYO-09 orange cryostat at HYSPEC.

The experiment was very successful in revealing the spurious-free scattering from the Orange cryostat, as well as several crystal field excitations that are different for both phases due to the different local symmetries.

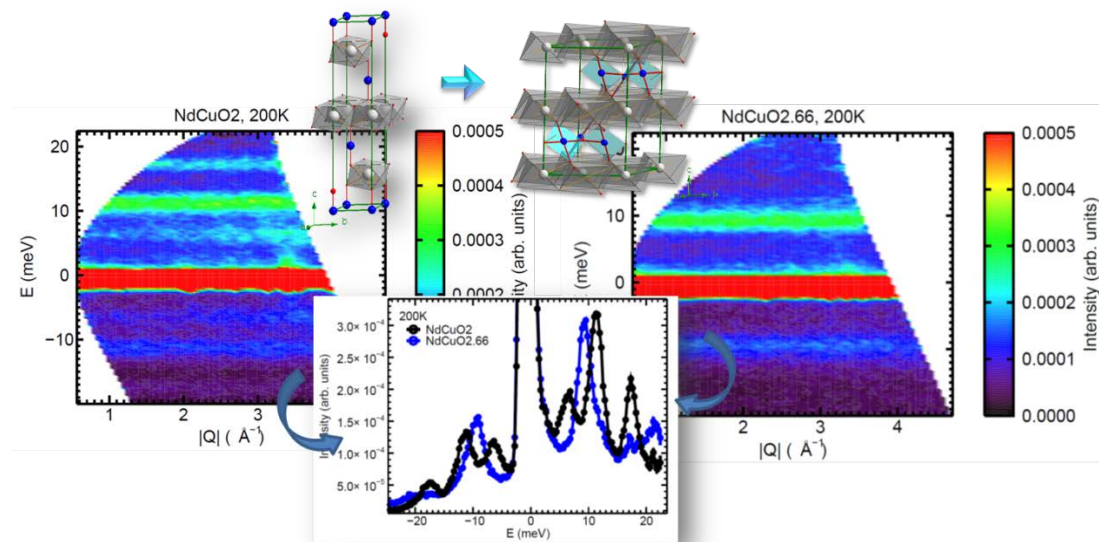


Figure: Changes in the crystal field spectra driven by modification in Nd environment caused by the presence of additional oxygen anions in the $CuO_{0.66}$ planes. These oxygen anions cap the triangular faces of the NdO_6 octahedra, leading to 7- or 8-fold coordination.

O. Garlea: MnV2O4 spinel (IPTS-8950, March 2013)

In the spinel MnV2O4, the octahedral site is occupied by the V3+ ion having two 3d electrons in threefold t2g levels. The tetrahedral site is occupied by the Mn2+ ion which is in the 3d5 high-spin configuration with no orbital degrees of freedom. Previous measurements showed the existence of two transitions to long-range ordered ferromagnetic states, the first collinear and the second noncollinear. The lower temperature transition, characterized by development of antiferromagnetic components in the basal plane, is accompanied by a tetragonal distortion and the appearance of a gap in the magnetic excitation spectrum.

The measurements at HYSPEC were performed on a crystal aligned in the (hk0) horizontal scattering, and were intended to map out the low-energy spin-wave branches along the principal directions. Measurements were successful in mapping the dispersion of the acoustic spin wave mode with the zone boundary energy of ~ 9 meV. Additional spin-wave branches that were expected to extend to energies of approximately 23 meV have not been detected.

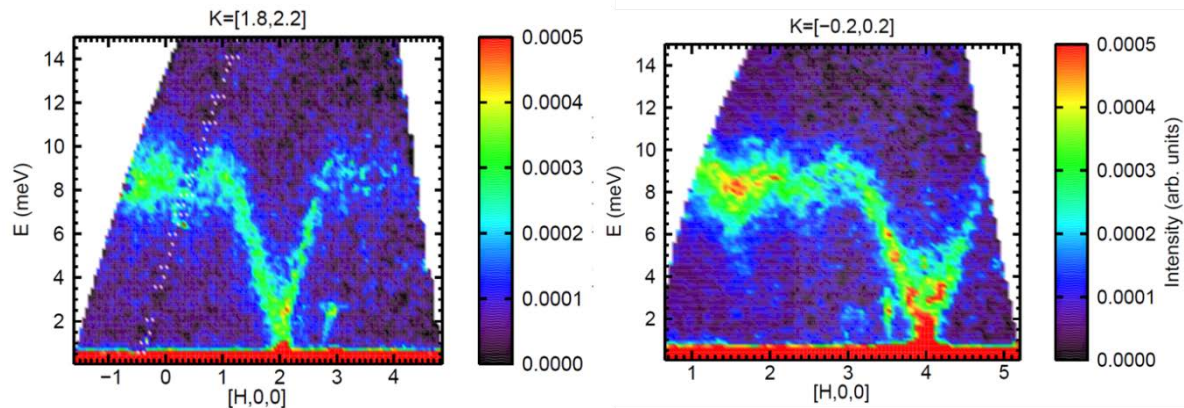


Figure: Low energy spin wave excitation spectrum of orbital-ordered spinel MnV2O4.

C. Li, O. Delaire: CrSb2 (IPTS-8562, April 2013)

CrSb₂ has gained recent attention as a narrow-gap semiconductor with potential thermoelectric properties. A surprising property of CrSb₂ is its highly anisotropic and unusual thermal conductivity, which appears for $T > 50$ K and reaches a maximum around 110 K, but the difference is still significant even at ambient temperature. It is believed that the magnons could contribute significantly to the thermal conductivity over a broad temperature range but the anisotropy could also result from the differences in magnon-phonon scattering in different directions. Phonon dispersions and linewidths of CrSb₂ were measured on HYSPEC at temperatures of 50~400K using a CCR and a stick furnace. The instrument and sample environments worked wonderfully during the experiment. The results are informative to gain the necessary insights into effective phonon scattering processes and benchmark microscopic theories of thermal conductivity.

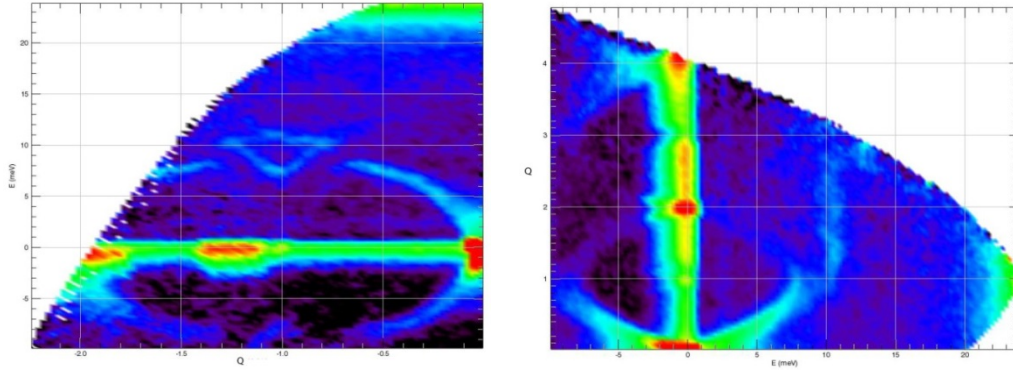


Figure: Transverse acoustic (TA) phonon dispersions of CrSb_2 along two high symmetry directions. Note their complex interactions with other phonon branches at the zone boundary. Low energy acoustic phonons are the dominating contributor for phonon thermal transport.

D. Fobes / I. Zaliznyak: $\text{Fe}_{1.06}\text{Te}$ (IPTS-8154 April 2013)

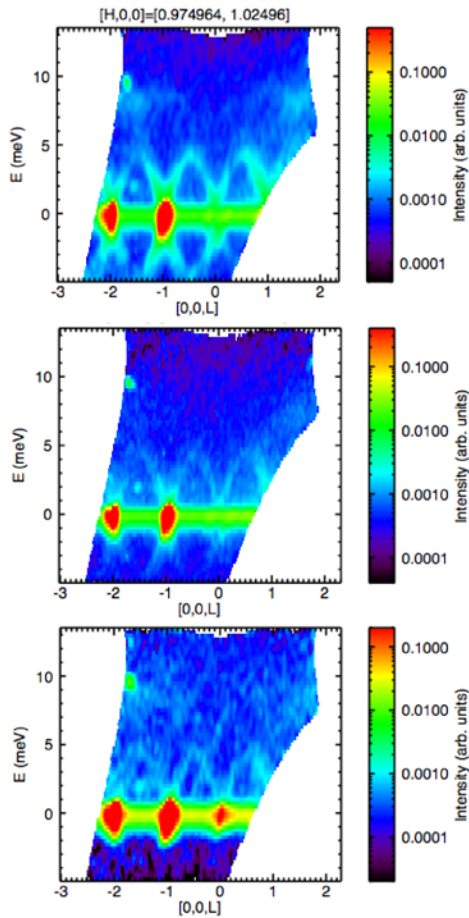


Figure: Temperature dependence of phonon-like modes emerging from (1 0 1) and (1 0 0) positions at (a) 300 K, (b) 80 K, and (c) 5 K (top to bottom) with $E_i=15\text{meV}$. Since there is no structural Bragg peak at (1 0 0) above the structure transition in this material ($\sim 65\text{K}$), the phonon-like mode emerging from this position is unexpected and requires more analysis.

The goals were to search for the low energy mode, and investigate the temperature dependence of the structural Bragg peaks and diffuse magnetic scattering, to investigate the effects of iron stoichiometry. We observed an unusual excitation emerging from a position where Bragg scattering is forbidden by structure factor.